RESEARCH ARTICLE

Protein Purification

Biotechnology Journal

www.biotechnology-journal.com

Modulator Dynamics Shape the Design Space for Stepwise-Elution Simulated Moving Bed Chromatographic Separations

*Chris J. Wayne and Ajoy Velayudhan**

For proteins and other biological macromolecules, SMB chromatography is best operated non-isocratically. However, traditional modes of non-isocratic SMB operation generate significant mobile-phase modulator dynamics. The mechanisms by which these modulator dynamics affect a separation's success, and thus frame the design space, have yet to be explained quantitatively. Here, the dynamics of the modulator (e.g., salts in ion exchange and hydrophobic interaction chromatography) are explicitly accounted for. This leads to the elucidation of two new design constraints, presented as dimensionless numbers, which quantify the effects of the modulator phenomena and thus predict the success of a non-isocratic SMB separation. Consequently, these two new design constraints re-define the SMB design space. Computational and experimental studies at the boundaries of this design space corroborate the theoretical predictions. The design of efficient and robust operating conditions through use of the new design space is also demonstrated.

1. Introduction

It is well known that, under isocratic conditions, SMB systems can efficiently produce output streams of high purity. This combination of high purity and high productivity is based upon two characteristics of the SMB layout: 1) The simulated countercurrent flow increases separation resolution relative to batch chromatography, and 2) the purity goal need not be fulfilled everywhere in the column series, but only at the two outlets (the extract and raffinate), thus enabling high sorbent utilization.[1]

1.1. Isocratic SMB Separations

For the application of a classic four-zone isocratic SMB to a binary separation problem, there are three well-known SMB design methods available to the investigator. Triangle Theory,[2–4] Standing Wave Design,[5,6] and Separation Volume Design[7] have all been applied to various separation challenges in the literature.

Of these three design methods, Triangle Theory is perhaps the most widely cited. Triangle Theory employs a graphical "flow-rate ratio" operation space, within which a triangular design space is delineated. Such a representation permits the investigator to choose liquid flow rates and switching times that are productive and robust to pump flow-rate variation.

All three of the established design methods can be used for the design of isocratic linear systems with both fast and slow mass transfer. Further, both Standing Wave Design and Triangle Theory have been adapted to design separations under non-linear isotherm conditions.[8,9]

1.2. Stepwise-Elution SMB (SE-SMB) Separations

In certain chromatography applications such as proteinaceous ion-exchange (IEX) separations, isocratic operation of countercurrent separations is rarely viable because of the "all or nothing" nature of feed retention as a function of the modulator concentration: a small change in modulator concentration can convert the very strong binding of macromolecules into very weak binding.[10,11] Process productivity may be improved through use of stepwise-elution programs for such systems; these programs form an SMB step "gradient" by a fixed desorbent modulator concentration (C_D) that is then diluted (or concentrated) by a different fixed feed modulator concentration (C_F).[12] SE-SMB schemes have been previously applied to various proteinaceous and small-molecule separation problems.[13–15]

Triangle Theory has been adapted to describe the design space in a flow-rate ratio graphical space for step-gradient TMB operation.[16,17] However, the TMB model of the SMB modulator profile is often inaccurate. TMB models fix the location of the modulator discontinuity at the feed point, but port switching in SE-SMB systems causes the modulator discontinuity to periodically lag behind the feed port in space. A consequence is that spatial inhomogeneities in the modulator concentration are generated which can span the entire closed-loop SMB column series. These inhomogeneities have been previously

C. J. Wayne, Prof. A. Velayudhan
Department of Biochemical Engineering
University College London
London, UK
E-mail: a.velayudhan@ucl.ac.uk

DOI: 10.1002/biot.201700664

observed experimentally,[18,19] and can be significant enough to make the step-gradient TMB-based Triangle Theory inaccurate. Consequently, separations based on Triangle Theory design can be substantially worse than expected.[20] It is therefore clear that the modulator needs to be treated as a separate species in the analysis of SE-SMB designs; such simulations have been presented previously.[21,22]

A fundamental understanding of these modulator variations is not, to the best of our knowledge, available in the literature. In this paper, we provide a detailed analysis of such modulator variations or "perturbations", and show how to design effective and robust separations in their presence. To this end, we introduce two new modulator-related dimensionless numbers, Υ and Ω, which can be used to characterize the design space. We demonstrate the importance of the new modulator design constraints experimentally by testing operation points which either just fulfill or just violate these constraints.

This paper also presents a new, more comprehensive approach to visualization of the design space for linear-isotherm fast mass-transfer SE-SMB systems by capturing all three control variables in a 3D design space. This representation permits the design of robust and productive systems that take into account the two new modulator-related design constraints. This design approach also facilitates robust and productive design of SE-SMB systems.

2. Theory

2.1. Comprehensive Design Space for SE-SMB

SE-SMB systems have three control variables per zone j; these are: 1) Liquid flow rate (Q_j), 2) Modulator concentration (C_j), and 3) Port-switching frequency (ω). A comprehensive graphical design space should span all possible values of these three control variables; we therefore propose a 3D $C_j/Q_j/\omega$ operational space. In such a space, plotting the (C_j, Q_j, ω) operation conditions for each zone results in four operational points for an open-loop four-zone system.

The following section details how this 3D framework may be used to design SE-SMB systems which meet the classic design constraints; Section 2.3 then uses this framework to design real SE-SMB systems that account for modulator dynamics.

2.2. Design of an Ideal SE-SMB

An ideal SE-SMB system differs from a real system, because it assumes there are no modulator perturbations (which are considered in the next section). Therefore, the only design constraints which apply to ideal SE-SMB systems are the four classical "flow-rate ratio" inequalities as well as solvent mass-balance equalities. This section describes these design constraints within the 3D operational space.

In SMB systems, both port switching and liquid flow proceed in the same "forward" direction (from left to right in **Figure 1**A). "Backward" movement of species in an SMB operation zone, therefore, is achieved when feed species move forward at a lower velocity than the port-switching velocity. Figure 1A summarizes how the differences between the port-switching velocity and the zonal velocities of feed species a&b (the two components of a binary feed mixture entering the system at "F") produce a binary separation in an SMB system.

There are a set of operational conditions that result in no net movement of a species, causing it to remain contained within a zone; we term these conditions "stationary operating conditions". These stationary operating conditions form surfaces in the $C_j/Q_j/\omega$ space, which become curves in the C_j/Q_j plane (for constant ω); such curves are shown in Figure 1C. There, the red curve represents the upper bound for the more-retained component (MRC), species "a", to move within a zone at a speed slower than that of the feed port. Similarly, the blue curve represents the lower bound for the less-retained component (LRC), species "b", to move within a zone at a speed faster than that of the feed port. The equations of these stationary curves are, by definition, an equivalence between the port-switching velocity (v_{ps}) and the feed species' velocity ($v_{i,j}$ for the "i"-th feed species in the "j"-th zone):

$$v_{i,j} = v_{ps} \tag{1}$$

Where v_{ps} and ω are related to the switching time (t_s) as follows:

$$\omega = \frac{1}{t_s} \tag{2}$$

$$v_{ps} = \omega \cdot L \tag{3}$$

For linear isotherms systems with fast mass transfer, the velocity of the feed species may be found by Solute Movement Theory (SMT), which predicts a species' zonal velocity ($v_{i,j}$) based upon its k_i' value, the zonal fluid flow rate (Q_j), and the total void fraction available to a species ($\varepsilon_{T,i}$).[23]

$$v_{i,j} = \frac{Q_j}{\varepsilon_{T,i} \cdot A_c \cdot \left(1 + k_i'\right)} \tag{4}$$

In SE-SMB systems, the k_i' value depends on the modulator concentration. In the example of IEX chromatography, this dependency may be described by the relation below.

$$k'_{i,C_j} = \varphi_i \cdot K_{0,i} \cdot e^{-S_i \cdot C_j} = k'_{i,0} \cdot e^{-S_i \cdot C_j} \tag{5}$$

This relation is similar to the algebraic dependence $k'_{i,C_j} = k'_{i,0} \cdot C_j^{-S_i}$ found in mass-action formulations.[24,25] Note that, for our purposes, an exponential decrease of binding with modulator is a simple and physically reasonable description; more complex behavior is sometimes seen experimentally.[26,27]

Combining the preceding equations results in the following equation for a stationary curve in the 3D operational space:

$$\omega = \frac{Q_j}{\varepsilon_{T,i} \cdot A_c \cdot L \cdot \left(1 + k'_{i,C_j}\right)} = \frac{Q_j}{V_{i,C_j}} \tag{6}$$

Therefore, in an ideal SMB system where V_{i,C_j} is the retention volume of species i at modulator concentration C_j in Zone j, the

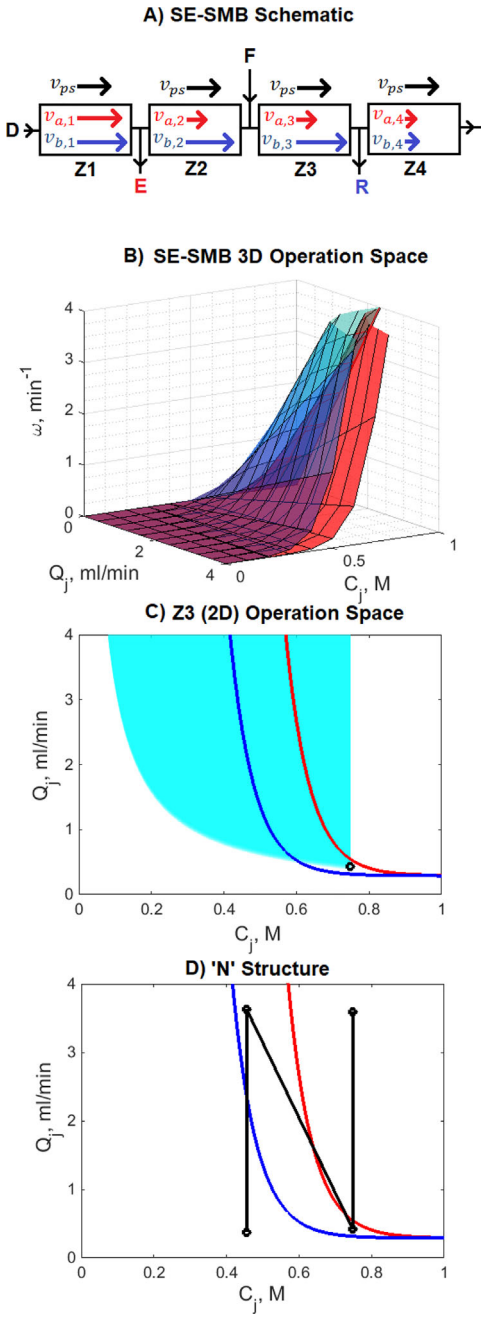

Figure 1. A) Differences between "forward" port-switching velocity (v_{ps}) and "forward" zonal feed species velocity ($v_{i,j}$), shown by arrows, effects the binary separation of two species (a&b) in a simulated counter-current system over time. Ports are labelled by initials D,E,F,R for Desorbent, Extract, Feed and Raffinate ports, respectively. Species "a" is more retained than species "b". B) Sequential Z2à Z3 design of an ideal SMB system. Stationary surfaces for the LRC and MRC are blue and red respectively. Z2/Z3 design space is enclosed by delineated by stationary surfaces in 3D SE-SMB design space. C) Choice of Z2 point (black) in design step 1 is used to delineate the Z3 operation space (cyan) with respect to physical constraints. The Z3 point must lie within the Z3 design space (between read and blue stationary curves) and within the cyan operation space. D) An "N" structure is formed from all four operation points. The Z1 and Z4 operation points lie above and below the MRC and LRC stationary curves respectively.

classical design constraints are inequalities limited by stationary operating conditions:

$$\frac{Q_1}{V_{a,C_1}} > \omega \tag{7}$$

$$\frac{Q_2}{V_{a,C_2}} < \omega < \frac{Q_2}{V_{b,C_2}} \tag{8}$$

$$\frac{Q_3}{V_{a,C_3}} < \omega < \frac{Q_3}{V_{b,C_3}} \tag{9}$$

$$\frac{Q_4}{V_{b,C_4}} < \omega \tag{10}$$

where:

$$C_1 = C_2 = C_D \tag{11}$$

$$C_3 = C_4 \tag{12}$$

$$Q_3 - Q_2 > 0 \tag{13}$$

Figure 1B shows the 3D ideal SMB design space. In this representation, the Zone 2 (Z2) and Zone 3 (Z3) operation points must lie within the space enclosed by the stationary curves (red and blue), whilst the Zone 1 (Z1) and Zone 4 (Z4) operation conditions must lie on either side of this enclosed space.

The 3D design space requires sequential choice of Z2 and Z3 operating points. This is because the initial choice of the Z2 or Z3 operation condition leads to constraints on the other through the solvent mass balance:

$$Q_3 \cdot C_3 = Q_2 \cdot C_D + Q_F \cdot C_F \tag{14}$$

where:

$$Q_F = Q_3 - Q_2 \tag{15}$$

Design of an ideal SE-SMB system through the 3D design framework would therefore occur as follows:

i) Select either Z2 or Z3 operation point in the 3D design space. Both of these operation points must lie within the stationary surfaces (red and blue in Figure 1B), but they cannot be chosen simultaneously. In this example, a Z2 operation point is chosen first. An efficient Z2 operation point has a low Q_2 to enable a high feed flow rate; this encourages selection of Z2 operation at low ω and high C_D.
ii) Since ω is set for all zones by the previous step, the 3D design space may be simplified to a 2D C_j/Q_j operation space. The remaining Z2 or Z3 operation point must be chosen in a physically-feasible region within the stationary

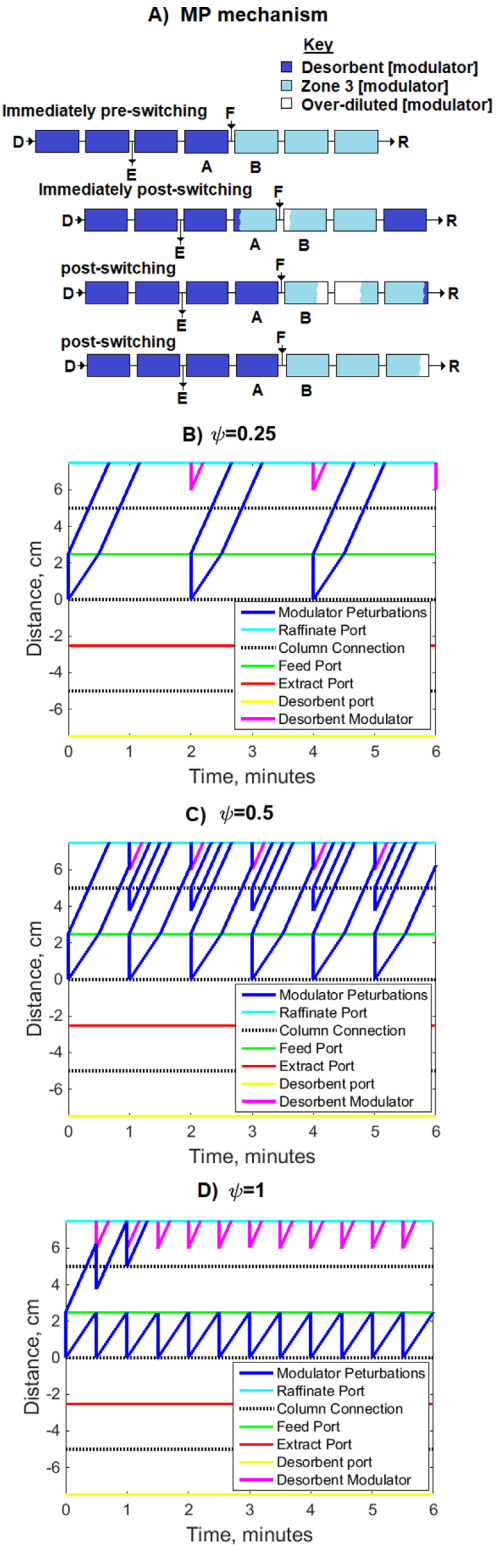

Figure 2. A) Illustration of the MP mechanism in an open-loop 3-Zone SMB system. Each row represents a time-progressive snapshot of the modulator concentration profile. Port switching occurs between the first and second rows of the diagram, which generates a MP pulse (white). B–D) Time distance diagrams of MPs (blue) in a 3-zone SE-SMB system run at various switching times: 2B) 2 min, 2C) 1 min, and 2D) 0.5 min.

curves. This feasible region, for the example of design beginning from the Z2 point, arises due to flow rate and modulator constraints ($Q_2 < Q_3 \leq Q_{max}$, $0 \leq C_F \leq C_{max}$) on the Z3 operation point. Given C_D was chosen in step 1, the solvent mass balance equation may be used to delineate the feasible Z3 operation space – in this case for a "step-down" ($C_3 < C_D$) process (cyan space in Figure 1C).

iii) The Z1 and Z4 operation points must be chosen to lie above and below the MRC and LRC stationary curves respectively. The Z1 and Z4 points must also be isocratic to the Z2 and Z3 points respectively. Once all points are chosen, drawing lines between the four points in sequence (Z1-Z4) should form an "N" structure (Figure 1D).

Figure 1C helps visualize how SE-SMB processes are capable of very high process productivity. Within the stationary curves, considerably more design space is available to maximize Q_F from the Z2 point when a step-down instead of an isocratic or "step-up" ($C_3 > C_D$) process is designed for this separation system.

2.3. The Modulator Perturbation Problem (MPP) in Real SE-SMB

In real SE-SMB systems, unlike in ideal models, modulator perturbations (MPs) occur. The MPP's mechanism is illustrated by **Figure 2**A, where a newly-concatenated column in Z3 ("A" in top row of Figure 2A) has a modulator concentration lower than that of the desorbent modulator concentration (assuming a step-down gradient). After port switching, the desorbent in this column is displaced into Z3, where further dilution by the feed stream occurs (white space, second row of Figure 2A). This MP is eventually cleared from Z3, as shown by rows 3&4 of Figure 2A.

A high switching frequency, or slow Z2 flow rate, can permanently depress the modulator concentration in the SMB. As shown by various distance time graphs in Figure 2, when the switching time becomes fast enough at a set Z2 flow rate the otherwise intermittent MP pulses (Figure 2B&2C) merge to produce perpetual and global over-dilution of the modulator in the post-feed zones (Figure 2D). In the extreme case, the MPP also leads to global over-dilution of the modulator in Z2 (not shown in Figure 2). Note that the starting modulator profile is from the expected TMB profile for the distance-time diagrams.

The MPP has two consequences for the design of SE-SMB systems. First, there is a need to prevent global over-dilution of both the Z2 and Z3 modulator profiles. The second consequence of the MPP is that it retards the migration velocity of species in Z3, and hence the classical design inequalities need modification to account for this aspect.

2.4. The First MP Constraint

The first MPP challenge is to design a SE-SMB where the post-feed modulator concentration equals the TMB model's concentration for at least part of every switching time's duration. This ensures that: 1) the modulator concentration in Z2 and Z3 does

not become globally depressed, and 2) any difference between the ideal and real Z2 modulator profile is contained to the final Z2 column. The first MP constraint thus permits duplication of the ideal SMB Z2 design constraints for real SMB systems, because feed species located a single column's distance away from the feed port experience the same duration of liquid flow at C_D as they would in the ideal SMB.

Global Z2 and Z3 modulator depression is avoidable by ensuring that the pulse of over-diluted modulator clears the end of the first post-feed column in Z3 before the next switching time. The first MP constraint may thus be derived by considering the time taken for the MP to clear first the final Z2 column (t_2), and then the first post-feed column (t_c):

$$t_2 = \frac{\varepsilon_{T,C_M} \cdot V}{Q_2} \tag{16}$$

$$t_c = \frac{\varepsilon_{T,C_M} \cdot V}{Q_3} \tag{17}$$

Where ε_{T,C_M} is the total void fraction available to the modulator. The first MP constraint is therefore the following inequality:

$$\frac{\varepsilon_{T,C_M} \cdot V}{Q_2} + \frac{\varepsilon_{T,C_M} \cdot V}{Q_3} < t_S \tag{18}$$

Literature reports of SE-SMB separations seem to acknowledge the first MP constraint implicitly, since the use of fast Z2 flow rates, low switching frequencies, and fast Z3 flow rates are common.

The small molecules often used as chromatographic modifiers typically exhibit significant axial dispersion; this makes the plug-flow assumption of equation 18 unrealistic. The first MP constraint thus needs amendment to account for the non-idealities of the modulator front. Since axial dispersion results in a larger equilibration volume requirement for a column exposed to a new modulator concentration, we can reform Equation (18) to be a function of this equilibration volume. The equilibration volume (V_{Eq}) is composed of the void volume of an SMB column combined with an additional experimentally-determined volume (V_{lag}) needed to complete a single column's re-equilibration to a new modulator concentration. Therefore, Equation (18) may be amended as follows in order to account for such non-ideality in salt-step migration:

$$V_{Eq} = \varepsilon_{T,C_M} \cdot V + V_{lag} \tag{19}$$

$$\frac{V_{Eq}}{Q_2} + \frac{V_{Eq}}{Q_3} < t_S \tag{20}$$

A harmonic mean flow rate (H_{Eq}) and a re-equilibrium flow rate (Q_{Eq}) may be used to simplify and express the first MP constraint (Equation (20)) as a dimensionless MP number (Ψ):

$$Q_{Eq} = \frac{V_{Eq}}{t_S} \tag{21}$$

$$H_{Eq} = \frac{2 \cdot Q_2 \cdot Q_3}{(Q_3 + Q_2)} \tag{22}$$

$$\Psi = \frac{2 \cdot Q_{Eq}}{H_{Eq}} \tag{23}$$

$$\Psi < 1 \tag{24}$$

Note that the first MP constraint requires determination of either the Z2 operation point (Q_2, C_2, t_s) or the Z3 operation point (Q_3, C_3, t_s) before the design space may be found for the other operation point. This is needed because the Z2 and Z3 flow rates influence the velocity with which the MP clears the first post-feed column relative to the port-switching velocity. Also, modulator mass-balance criteria necessitate sequential zonal design akin to the ideal SE-SMB design process.

For the design of a Z2 operation point in the 3D design space (mentioned in section on 1), the first MP constraint may be used curtail the ideal SMB design space to the real Z2 design space. Since there is a maximum column or pump flow rate (i.e., max $(Q) \geq Q_3$), a constraint on Q_2 may be derived from Equation (20):

$$\frac{V_{Eq}}{\max(Q)} \leq \frac{V_{Eq}}{Q_3} < t_S - \frac{V_{Eq}}{Q_2} \tag{25}$$

thus:

$$Q_2 > \frac{V_{Eq} \cdot \max(Q)}{\max(Q) \cdot t_S - V_{Eq}} \tag{26}$$

This constraint (Equation (26)) ensures that any chosen Z2 operation point will define a feasible Z3 design space; its effects on the Z2 design space are contrasted with the ideal Z2 design space in **Figure 3**A. Other 3D images which contrast the ideal and real SE-SMB design space (as in Figure 3A) may be found in the supplementary material.

2.5. The Second MP Constraint

MPs can retard the migration of species in Z3 independently of a global modulator depression scenario. Severe modulator perturbations result in the LRC accumulating in the system, which in experimental systems would result in overload conditions that can compromise product yield or purity. Ideal SMB design constraints do not account for such effects.

To model the impact of the MP on the feed species, we can conservatively assume that the MP concentration profile, which is smooth between the transitional modulator concentration of the MP pulse ($C_{\ddagger}$) and C_3, can instead be approximated by a square wave. Assuming that the first MP constraint is met, SMT can then be used to describe the total distance travelled by a feed species which experiences both a period of liquid flow at C_3 and liquid flow during the MP pulse at $C_{\ddagger}$, which is determined as

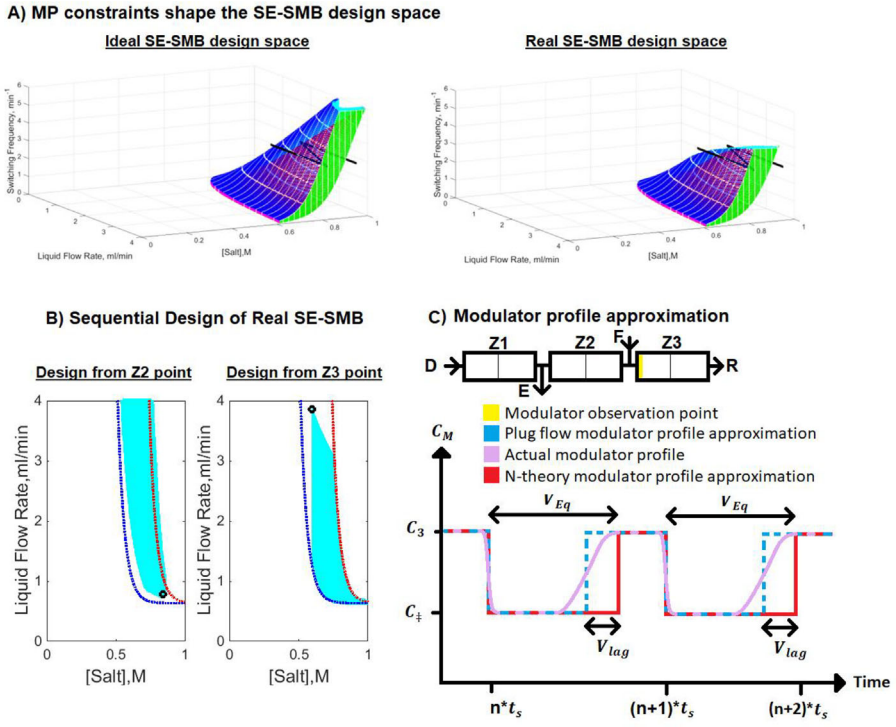

Figure 3. A) Comparison of ideal and real SE-SMB 3D Z2 design spaces for the same example "N" operation set. B) For a given switching time, prior determination of either the Z2 operation point (LHS) or Z3 operation point (RHS) differently shapes the solvent mass balance and Ω_i-shaped operation window (cyan). C) Comparison of the true modulator profile (smooth mauve line) to the conservative square wave (solid red line) V_{lag}-approximation immediately post-feed point.

follows:

$$C_{‡} = \frac{Q_2 \cdot C_3 + (Q_3 - Q_2) \cdot Q_2 \cdot C_F}{Q_3} \tag{27}$$

The duration of a species exposure to liquid flow at either $C_{‡}$ or C_3 is determined by the Z2 operation conditions. The $C_{‡}$ flow duration is equal to the time (t_2) needed for the C_D modulator front in Z2 to "catch up" with the moved Feed inlet port. This MP pulse period sums with the C_3 liquid-flow period to equal one switching period. Therefore, the total distance (x_i) travelled by a feed component per switching time in Z3 may be formulated as follows:

$$x_i = (t_S - t_2)\left(\frac{Q_3}{\varepsilon_{T,i} \cdot A_c \cdot (1 + k'_{i,C_3})}\right) + t_2\left(\frac{Q_3}{\varepsilon_{T,i} \cdot A_c \cdot (1 + k'_{i,C_{‡}})}\right) \tag{28}$$

where "$k\prime_{i,C_{‡}}$" is the k prime value at the transitional modulator concentration. Given that design of Z3 operation conditions requires that x_b and x_a are greater and lesser than one column's length respectively, the second MP Z3-design constraint may thus be derived:

$$\left(\frac{(t_S - t_2) \cdot Q_3}{\varepsilon_{T,a} \cdot A_c \cdot (1 + k'_{a,C_3})}\right) + \left(\frac{t_2 \cdot Q_3}{\varepsilon_{T,a} \cdot A_c \cdot (1 + k'_{a,C_{‡}})}\right) < L < \left(\frac{(t_S - t_2) \cdot Q_3}{\varepsilon_{T,b} \cdot A_c \cdot (1 + k'_{b,C_3})}\right) + \left(\frac{t_2 \cdot Q_3}{\varepsilon_{T,b} \cdot A_c \cdot (1 + k'_{b,C_{‡}})}\right) \tag{29}$$

where:

$$t_2 = \frac{\varepsilon_{T,C_M} \cdot V + V_{lag}}{Q_2} = \frac{V_{Eq}}{Q_2} \tag{30}$$

Equation (29) may be simplified with the use of two new dimensionless numbers $(\Omega_a \Omega_b)$ to the following:

$$\Omega_b < 1 < \Omega_a \tag{31}$$

where:

$$\Omega_b = \frac{Q_2}{Q_3}\left(\frac{V_{b,C_3} \cdot V_{b,C_?}}{(Q_2 \cdot t_s - V_{Eq}) \cdot V_{b,C_{‡}} + V_{b,C_3} \cdot V_{Eq}}\right) \tag{32}$$

$$\Omega_a = \left(\frac{Q_3}{Q_2}\right)\left(\frac{(t_s \cdot Q_2 - V_{Eq}) \cdot V_{a,C_3} + V_{Eq} \cdot V_{a,C_{‡}}}{V_{a,C_{‡}} \cdot V_{a,C_3}}\right) \tag{33}$$

Thus Equation (31) is the SMB design inequality for Z3. The second MP constraint means that the Z3 operation window is determined by modulator dynamics generated by

the Z2 operation conditions. The effect of Ω_a on the design space is shown by the left-hand side of Figure 3B; the additional design space conferred by the theoretical second MP constraint with respect to the ideal model is between the red stationary curve and the upper edge of the cyan design space. In the same figure, the second MP constraint (as a function of Ω_b) is responsible for the discrepancy between the ideal blue stationary curve and the lower edge of the cyan design space.

The Z4 SMB design constraint is derived very similarly to the Z3 design constraints, but requires that x_b is less than one column's length in this zone.

$$Q_4\left(\frac{(V_{b,C_\ddagger}(t_S - t_2) + t_2 \cdot V_{b,C_3})}{V_{b,C_3} \cdot V_{b,C_\ddagger}}\right) < 1 \tag{34}$$

It should be noted that a consequence of the square-wave approximation of the modulator profile is that the second MP constraint is slightly more strict concerning the LRC, and slightly more lax concerning the MRC, than experimentally-determined MP constraints. This is because proteins migrate further at the intermediate modulator concentrations between the smooth transition from $C_\ddagger$ and C_3 than if they were only subject to a discrete $C_\ddagger$ pulse. Whilst a more accurate migration distance of the proteins may be estimated by other means, such analysis is not as simple as the approach detailed above. Furthermore, the consequences of the square-wave modulator-pulse simplification are of little practical concern. Concerning the MRC-part of the second MP constraint, only SE-SMB designs which seek to minimize the modulator step risk accidental pollution of the raffinate.

2.6. Design of Real SE-SMB Operations

As derived by the preceding section, for a successful 4-zone stepwise-elution separation, the following design inequalities must be satisfied:

$$\frac{Q_1 \cdot t_s}{V_{a,C_1}} > 1 \tag{35}$$

$$\frac{Q_2 \cdot t_s}{V_{a,C_2}} < 1 < \frac{Q_2 \cdot t_s}{V_{b,C_2}} \tag{36}$$

$$\Psi < 1 \tag{37}$$

$$\Omega_b < 1 < \Omega_a \tag{38}$$

$$Q_4\left(\frac{(V_{b,C_\ddagger}(t_S - t_2) + t_2 \cdot V_{b,C_3})}{V_{b,C_3} \cdot V_{b,C_\ddagger}}\right) < 1 \tag{39}$$

Given that both the Ψ and Ω_i numbers shape the design space for the Z2 or Z3 operation point based upon known Z3 or Z2 conditions, respectively, the real SMB design process is unavoidably sequential. It is thus amenable to the design process outlined for the ideal SMB system described in section 1. Figure 3B shows how the real SMB operation space (cyan) is determined for the one of the Z2 or Z3 points given prior selection of the other. As can be seen, the design space for the Z2 point is coterminous with the stationary curves from the ideal SMB, while the design space for the Z3 point is not due to the MPP. For this reason, we propose sequential design should generally begin from the Z2 operation point. Note that the first MP constraint is not delineated in Figure 3B.

2.7. Design of Robust and Productive SMB Operations

Framing the operation space in terms of the three SE-SMB control variables permits scrupulous design of robust SMB processes. The effects of common SMB failure modes such as modulator concentration variations, ligand loss from columns, and pump flow-rate variability, may be mapped in the design space. Robust processes may thereby be designed.

In the event of ligand loss, the virtual solid flow-rate is effectively reduced. This would displace all four operation points of the "N" down the switching frequency axis, since the switching time would effectively increase – though without mollifying the first MP constraint. The choice of SMB operation conditions that permit transposition of the operational "N" toward slower switching frequencies – whilst still satisfying the design constraints – is necessary in the design of a process robust to ligand loss.

Robust design of SMB processes must also include robustness to pump flow-rate variations and modulator variations. Minor pump flow-rate variations translate into modulator concentration changes, which can be particularly dangerous for SE-SMB given the often-exponential binding dependence of modulator concentration. Also, modulator concentration in the desorbent and feed steams may suffer minor variances. It is possible in the 3D design space to draw operation lines which map each of these eventualities.

Apart from aiding robust design, the 3D design method facilitates graphical optimization of fast mass-transfer separation systems. Process productivity may be improved by exploiting a step gradient in the modulator concentration to maximize Q_F. Therefore maximization of the vertical and horizontal distances between the Z2&Z3 operation points on the C_j/Q_j axes is an intuitive local optimization method. Furthermore, desorbent usage may be locally optimized by choosing Z1&Z4 operation points close to the MRC and LRC stationary curves respectively.

3. Experimental Section

3.1. Computational

A standard 3-Zone SMB model, based upon lumped axial dispersion and solid-phase linear driving force (LDF) mass transfer, was constructed. In addition to this, another common

Table 1. Properties of model system used in SMB experiments.

Parameter	Parameter value
$k'_{a,0}$ (lysozyme)	1.75e4
S_a (lysozyme)	14.2
$\varepsilon_{T,a}$	0.54
$k'_{b,0}$ (β-Lactoglobulin)	8e4
S_b (β-Lactoglobulin)	22.6
$\varepsilon_{T,a}$	0.52
ε_{T,C_M}	0.86
V_{lag}, mL	0.4
Individual column dimensions, cm	2.5 × 0.7 i.d.
Maximum liquid flow rate, mL min^{-1}	4

model that used a liquid-phase LDF formulation was constructed. Details of these two standard models may be found in Refs. [5,28], and literature examples of the two models' application to describe SMB systems (including initial and boundary conditions) include the following references.[5,29] Model details are also included in the supplementary material. The modulator dynamics were simulated by modelling it as an unretained third component in the SE-SMB system.

To solve the model equations, discretization of the convective term was carried out using a first-order, upwind-differencing, finite-volume method. The diffusive term was discretized using the first-order central-differencing method; mirror nodes were included at the ends of each simulated column. 90 nodes per column were used, and the differential algebraic equations (DAEs) were solved by Matlab's ode15s; a stiff multi-step solver based on backward differentiation formulas. To simulate sequential port switching in the SMB, the ordinary differential equation starting conditions (i.e., the concentration profiles of the proteins and modulator in the system found after solving for the previous switching interval) were shifted counter-current to the liquid-flow direction by one column's number of nodes after every switching period.

For both simulation models, the equilibrium concentration of a species in the solid phase was described by a linear isotherm with exponential decay by increasing modulator concentration, as given by Equation (5).

3.2. Experimental

An Octave SMB device (Semba Biosciences, Wisconsin USA), and HiTrap SP FF 1mL (2.5 × 0.7 cm i.d.) cation exchange columns (from G.E.), were used for all SMB experiments. Each experiment's configuration and number of columns per zone is detailed in the results tables.

All experiments used a 25 mM solution of citric acid − trisodium citrate buffer, pH 3.8. Sodium chloride was added appropriately to control salt concentration. All buffer materials and proteins were purchased from Sigma–Aldrich UK. Lysozyme and β-Lactoglobulin A&B were >90% pure and combined to form a binary feed mixture.

An AKTA PURE system (from G.E.) was used to determine the equilibrium binding parameters of Lysozyme and β-Lactoglobulin A&B. The buffer conditions used promoted dimerization of the β-Lactoglobulins.[30] These dimers were treated as one protein species. Isocratic runs of Lysozyme and β-Lactoglobulin were performed at a variety of different salt concentrations with a 4mL (10 cm by 0.7 cm i.d.) HiTrap SPFF, at a flow rate of 2 mL min^{-1}. Matlab was used to fit the linear isotherm coefficients (S_i and $k'_{i,0}$) to the data, as shown by **Table 1**.

Parameter estimation of the total void fraction available to both the modulator (ε_{T,C_M}) and the proteins ($\varepsilon_{T,i}$) was conducted with a 10ml (25 cm by 0.7 cm i.d.) HiTrap SPFF column at a flow rate of 2 mL min^{-1}. These parameters were found using the method employed in Ref. [21]. V_{lag} was defined as the volume between 50 and 100% conductivity breakthrough for a modulator step to reach the end of one SMB column.

The Wilson-Geankoplis correlation was used to determine the external film mass-transfer coefficient of the experimental proteins.[31] The protein's diffusivity was found using the Young et al. correlation.[32] The lumped axial-dispersion term was then

Table 2. Experiment to demonstrate the first MP constraint.

	Experiment 1 (**Figure 4**A left)	Experiment 2 (Figure 4A right) Parameter value
Parameter	Violation of first MP constraint (dashed magenta system)	System robust to first MP constraint (green system)
Extract Purity	≈50%	>98%
Raffinate Purity	>98%[a)]	>98%
Q_2 (Ψ), mL min^{-1}	0.58	0.57
Q_2, mL min^{-1}	0.56	0.75
ψ	1.06	0.70
Ω_b	0.37	0.27
Ω_a	0.47	0.53
Q_E, mL min^{-1}	1.54	1.26
Fixed Parameters	Q_D, 2.1 mL min^{-1}; Q_F: 2.8 mL min^{-1}; C_D: 0.56 M; C_F: 0.42 M; Column configuration: 3-2-3; t_s: 2.5 min; Feed components: 1 mg mL^{-1} lysozyme & 1 mg mL^{-1} β-Lactoglobulin	

[a)]Significantly reduced yield of raffinate product.

Table 3. Properties of simulated system used to demonstrate the second MP constraint; **Figure 4**B.

Experiment number/Parameter	1	2	3	4	5
System position in Figure 4B	Left most	2nd from left	3rd from left	2nd from right	Rightmost
Inside/Outside real SMB design space?	In	In	In	Out	Out
Reached cyclic steady state? (Y/N)	Y	Y	Y	N	N
Ω_b	0.94	0.97	0.99	1.01	1.06
Ω_a	0.98	0.68	0.56	0.54	0.41
ψ	0.21	0.29	0.36	0.36	0.52

determined using the Chung and Wen correlation.[33] These parameters facilitated employment of liquid-phase LDF SE-SMB model to investigate the behavior of the experimental protein separation in silico, and are detailed in the supplementary data.

The AKTA PURE was used to analyze SMB outlet purity offline. Samples (0.5 mL) were loaded on a 5 mL HiTrap SP FF column ($10 \times 0.7\ cm^2$ i.d.) column, and subject to a 375–700 mM NaCl gradient over 10 CVs. Similar conditions were used to produce the chromatogram in **Figure 4**D, except a 2 mL HiTrap SPHP ($5 \times 0.7\ cm^2$ i.d.) was used with a flow rate of 1 mL min^{-1}, load volume of 100 µL, and feed mixture from experiment 1 in **Table 4**.

All SMB experiments used back pressure regulators of 250 psi on the Extract pump, 100 psi on the raffinate pump, and 40 psi on both the feed and desorbent pumps. Separations were run until the UV 280 nm signals from the extract and raffinate indicated cyclic steady state had been reached, which typically meant a 2 h run.

4. Results

4.1. The Effects of the MP Constraints on the Design Window

A set of experiments were used to test the first MP constraint from a chosen Z3 operation point. Figure 4A shows the two experimental operating conditions of a 3-zone model binary separation system of Lysozyme (MRC) and β-Lactoglobulin A&B (LRC), where the first MP constraint is delineated graphically as the lower bound for Q_2 (solid black line). The operating points form a "V" instead of an "N" because there is no fourth zone. The LHS separation (dashed magenta system) in Figure 4A failed because its Z2 operation point violated the $Q_2(\Psi)$ constraint, whilst RHS green system permitted a successful separation as it satisfied this constraint (details in **Table 2**).

To test the second MP constraint computationally, SE-SMB simulations using a hypothetical system were performed. These simulations are described in **Table 3**; additional details may be found in the supplementary data). The operation window was framed using a pre-selected switching time and Z3 operation point (blue scatter point). As shown in Figure 4B, a set of different 3-zone SMB operating conditions on either side of the $Q_2(\Omega_b)$ boundary (black curve) were simulated. Z2 operation points superior to the $Q_2(\Omega_b)$ constraint (green systems) reached a cyclic steady state during a simulated 24 h process run time, whilst the dashed magenta systems conditions did not; the LRC accumulated in these systems. In Figure 4B, the $Q_2(\Psi)$ constraint is outside of the displayed design space, and the Z1 operation points are also not shown.

Further experiments were used to demonstrate the discrepancy between the ideal and real SMB design spaces. These experiments were designed from a pre-selected switching time and Z2 operation point. As shown in Figure 4C, and detailed in Table 4, Z3 operation conditions that both resulted in pure separations and reached cyclic steady state always occurred

Table 4. Operation conditions used to demonstrate MP constraint boundaries; **Figure 4**C.

Parameter	Experiment 1	Experiment 2	Experiment 3	Experiment 4	Experiment 5	Experiment 6
System position in Figure 4C	Left-most	2nd from left	3rd from left	3rd from right	2nd from right	Right-most
Inside/Outside real SMB design space?	Out	Out	Out	In	In	Out
Extract Purity	≈50%	≈70%	≈80%	>98%	>98%	>98%[a)]
Raffinate Purity	>98%[a)]	>98%[a)]	>98%[a)]	>98%	>98%	≈50%
Ω_b	8.22	2.66	1.19	0.38	0.23	0.13
Ω_a	0.03	0.06	0.11	0.29	0.49	1.01
ψ	0.42	0.42	0.42	0.42	0.42	0.42
C_F, M	0	0.125	0.215	0.35	0.42	0.52
Fixed parameters	t_s: 2.5 min; Column configuration: 4-2-2; Q_D: 4 mL min^{-1}; Q_E: 2.5 mLmin^{-1}; Q_F: 1 mL min−1[1]; C_D:0.52 M; Feed components: 1 mg mL^{-1} lysozyme & 1 mg mL^{-1} β-Lactoglobulin					

[a)]Significantly reduced yield of protein from outlet port.

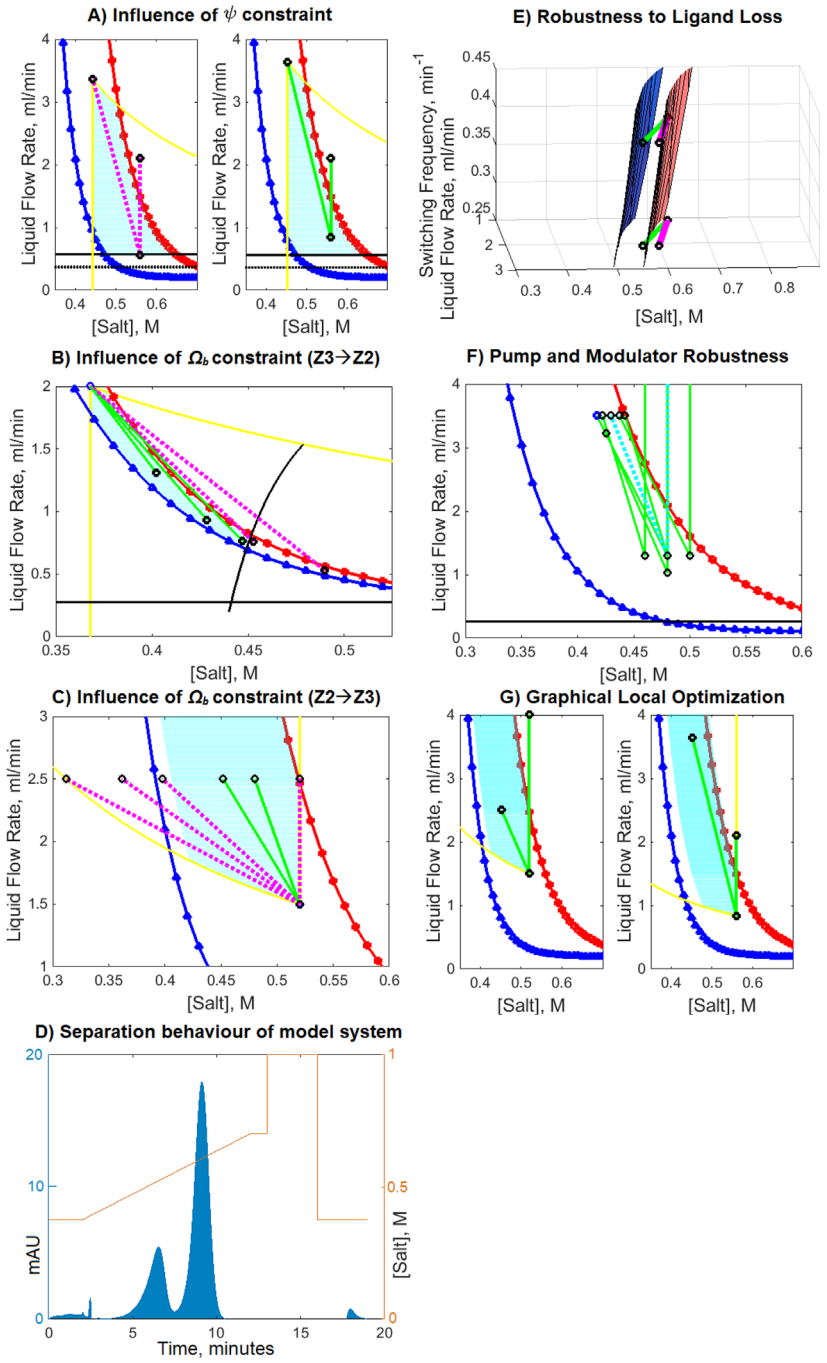

Figure 4. Sub-figures A,B,C,G: Design spaces (cyan) formed from either the Z2 or Z3 operation point, the MRC (red squares) and LRC (blue triangles) stationary curves, and the "step-down" C_D or C_F modulator limits (yellow curves & lines) A) Two experiments to test the first MP $Q_2(\Psi)$ constraint (shown by solid black lines); the dashed black lines show the $Q_2(\Psi)$ constraint for the hypothetical case that $V_{lag} = 0$. The two sets of operation conditions are shown by either green or dashed-magenta "V" shapes. B) Various SE-SMB operating conditions (Z2&Z3 operation points joined by either dashed-magenta or green lines) were simulated either side of the $Q_2(\Omega_b)$ constraint (black curve) to test this constraint. C) Various Z3 conditions were used to experimentally test $Q_3(\Omega_i)$ design window validity. Each experiment's Z2&Z3 operation point is joined by either dashed-magenta or green lines. D) Experimental batch-gradient chromatogram showing the model proteins' separation behavior. E) 3D view of two SE-SMB systems (green and magenta) at two different switching frequencies; the two green and magenta operation points on the lower switching frequency plane model the effects of ligand loss on the 3D operation set. Stationary surfaces are red (MRC) and blue (LRC). F) Experiments inside design space to demonstrate robust design of an SE-SMB separation. Black line represents $Q_2(\Psi)$ constraint, stationary curves are red with squares (lysozyme) and blue with triangles (β-lactoglobulin). The $Q_2(\Omega_b)$ constraint is outside of the displayed area. Green "V" systems represent processes run at [salt] or flow-rate deviations away from original process set-point (cyan-dashed "V" system). The $Q_2(\Omega_b)$ constraint applies to the most MPP-unfavorable Z3operation point (blue scatter point) and is outside the displayed operation space. G) Productive SE-SMB design through the new design method. Left: Original separation operational conditions, Right: Improved operational conditions.

within the real SE-SMB design window (cyan), but not always within the ideal SE-SMB design window (framed by the stationary curves). The relative positions of the experimental operation points – with respect to the $Q_3(\Omega_b)$ design space boundary and stationary curves – were robust to ±5% variation in the $\varepsilon_{T,i}$ values.

4.2. Robust and Productive SE-SMB Operation Design

Computational simulations and experiments were used to explore the effectiveness of robust design in the new design space for various scenarios including ligand loss, inlet modulator-concentration variances, and liquid flow-rate variation.

Ligand loss leads to raffinate pollution and the attendant recovery loss of extract product, so robust design must primarily focus on the Z3 operation point. To show that ligand loss may be modelled as a virtual decrease in switching frequency, computational simulations (described in supplementary material) were performed. In these simulations, Z3 consisted of three columns which were simulated to have lost 33% of their ligand each. Therefore, the port-switching frequency in Z3 was effectively two thirds of the original frequency (for one switching period in an eight-column system). Figure 4E shows the stationary surfaces in the 3D design space, where – for this system – the MRC stationary surface is a very close approximation of the $Q_3(\Omega_a)$ constraint. It was shown by simulation that the (green) Z3 operation point within the stationary surfaces was robust to ligand loss, whilst the (magenta) Z3 point outside these boundaries suffered from periodic pollution of the raffinate by the MRC, as predicted. A simulation where two columns lost 50% of their ligand, and the $K_{0,i}$ values for species halved accordingly, showed the same vulnerability to raffinate pollution, since Z3 experienced an identical decrease in apparent port-switching velocity (data not shown). Note that if all columns experience ligand loss, but the Z3 and not the Z2 operation point is robust, then the Z2 operation point must also to be moved within the ligand loss stationary curves or risk accumulation of the MRC around the feed which would lead to poor extract recovery and/or competitive binding behavior.

Robust design of SMB processes also anticipates pump flow-rate and inlet modulator-concentration variations. To demonstrate the utility of the new design space for design of SMB processes robust to such variations, a set of "worst-case-scenario" binary separations were performed in which process conditions were perturbed away from the set-point operating conditions.

The robust set-point process condition (dashed-line cyan system, Figure 4F; experimental details in supplementary material) was found by first assuming that the feed flow-rates of all systems would exceed their Z2 flow-rates. This meant that C_3 would have greater sensitivity to C_F than C_D modulation. Since the $Q_2(\Omega_b)$ constraint is more dependent on C_3 than Q_3 in these systems, the robust set-point process conditions were found by first drawing the Z3 operation point for the C_F-increase perturbation system (Figure 4F, blue point). This system has the most limiting $Q_2(\Omega_b)$ constraint, so other systems may be subsequently drawn that are guaranteed safe from violating the second MP constraint as it applies to the LRC. Once this set-point system was chosen, various failure-mode conditions were explored. Extract and raffinate purities were all greater than 90% and hence robust to the process perturbations explored.

To demonstrate productive design within the new design framework, a pair of experiments were performed (experimental conditions detailed in supplementary material). An original separation process ("V" operation set in LHS of Figure 4G) was improved by increasing the feed flow rate, which loosened the MP constraints on the Z3 design space (cyan space,Figure 4G RHS). The desorbent flow rate was also reduced in the improved process by bringing the Z1 operation point closer to the MRC stationary curve, thus reducing desorbent utilization (Q_F/Q_D). This graphical "local optimization" led to an increase in product-specific sorbent utilization from 0.25 to 1.33 $g\,L^{-1}\,h^{-1}$.

To demonstrate that the true design space of the experimental protein separation is justifiably approximated by the design space shown in Figures 4A, 4C, 4F, & 4G – which assumes very fast mass-transfer – further simulations were performed. Using the liquid-phase LDF SE-SMB model with parameters from Table 1 and the supplementary data, each successful experiment (green systems in Figures) was replicated in silico. Additional simulations, which used a fast mass transfer rate ($k_{f,i} = 20\,s^{-1}$) were also performed. There was complete agreement between all theoretical predictions, experimental results, and simulations results.

5. Discussion

This paper proposes a unified design space in the three SE-SMB zonal control variables: liquid flow rate, modulator concentration, and switching frequency. Accounting for the detailed dynamics of the modulator then led to the development of the dimensionless numbers, Ψ and Ω_i, which further shape the design space to permit successful SE-SMB separations. Experimental and simulation data was presented to show the practical importance of Ψ and Ω_i. While these dimensionless numbers were explored here for IEX separations, they may be generalized to different SE-SMB systems and other modulator-determined partitioning relationships. It may also be possible to adapt Ψ and Ω_i to aid design of non-conventional SE-SMB operating schemes (e.g., in Refs. [34–36]). However, MP phenomena do not occur in most multi-column batch processes (e.g., in Ref. [37]).

It could be argued that investigators should avoid the use of the Ψ and Ω_i numbers by simply employing a very low switching frequency. The design space is less restricted by the MPP under such conditions (see Figure 3A). Also, such systems can be highly productive, because the feed flow rate may be much larger than that permitted by higher switching frequencies. However, there are drawbacks to this approach. A slower switching frequency leads to: 1) longer start-up times, 2) reduced process robustness to ligand-loss, 3) a slower feedback loop for SMB control engineering [Wayne, C.J., Velayudhan, A., Continuous Biomanufacturing Conference, University of Oxford, June 2017], and 4) ceteris paribus, a greater chance of overload conditions occurring in systems, which can lead to reduced purity and recovery in SE-SMB processes where system design assumes only linear-isotherm behavior.

This paper has presented simulation results to show that, for linear-isotherm systems with fast mass transfer, there are predictable consequences of violating the MP design constraints. When $\Omega_a < 1$, pollution of the raffinate results, whereas when

$\Omega_b > 1$, there is accumulation of the LRC in the system as the raffinate yield is compromised. If $\Psi = 1$, global over-dilution of Z3 will result, while if $\Psi > 1$, this over-dilution will extend to all of Z2. Depending on the size of the modulator step used in the system, the consequences of violating the first MP constraint span from reduced raffinate yield due to LRC accumulation (as Z3 modulator depression triggers violation of the second MP constraint), to pollution of the extract (when $\Psi > 1$), as the traditional Z2 design constraint is violated.

For the protein-protein separation system investigated, there was complete agreement between the theoretical predictions, experimental results, and simulations results. Therefore the design space we constructed theoretically for fast mass transfer is in agreement with the simulations performed for the appropriate mass transfer rates, as well as with the experimental results. We thus conclude that our theoretical design space is applicable to these protein separations. Naturally, for sufficiently large proteins, a suitable adjustment will have to be made because the mass transfer rates will become very low; this adjustment is not discussed here. Nevertheless, it is important to note that the current theory is quantitatively correct for small molecules such as sugars and enantiomers, as well as moderately sized proteins (with molecular mass less than 30kDa), and is therefore useful for many SMB separations of practical interest.

For nonlinear systems, and systems with slow mass transfer, the consequences of violating the MP constraints have yet to be investigated. Unfortunately, design of these systems must currently rely on detailed SMB modelling, since no comprehensive SE-SMB design space exists. To address this issue, our future contributions will seek to refine the 3D design space to account for the modulator perturbations, slow mass-transfer, and competitive binding behavior which is typical of industrially-relevant separation problems.

Abbreviations

IEX, Ion-Exchange; LHS, Left Hand Side; LRC, Less retained Component; MP, Modulator Perturbation; MPP, Modulator Perturbation Problem; MRC, More Retained Component; RHS, Right Hand Side; SE-SMB, Stepwise-elution SMB; SMB, Simulated Moving Bed; SMT, Solute Movement Theory; Z1, Zone 1; Z2, Zone 2; Z3, Zone 3; Z4, Zone 4.

Supporting Information

Supporting Information is available from the Wiley Online Library or from the author.

Acknowledgements

Prof. Ajoy Velayudhan acknowledges an Engineering and Physical Sciences Research Council (EPSRC) manufacturing fellowship for macromolecular manufacturing. The authors would also like to acknowledge the support of the Centre for Doctoral Training at the Department of Biochemical Engineering at University College London.

Conflict of Interest

The authors declare no commercial or financial conflict of interest.

Nomenclature

A_C [cm^2] Column cross-sectional area
$C_‡$ [M] Modulator concentration in MPP pulse
C_D [M] Modulator concentration in desorbent solution
C_F [M] Modulator concentration in feed solution
C_j [M] Modulator concentration in zone j
D_i [m^2 $second^{-1}$] Axial dispersion coefficient for species i or the modulator
F_i [$mLmin^{-1}$] Feed solution concentration of species i
H [$mLmin^{-1}$] Harmonic mean of liquid flow rates in Zone 2 & Zone 3
$k_{m,i}$ [$second^{-1}$] Solid Phase mass-transfer rate coefficient
$k_{f,i}$ [$second^{-1}$] Liquid Phase mass-transfer rate coefficient
$K_{0,i}$ [−] Partition coefficient at 0M modulator for species i
k'_{i,C_j} [−] k prime value for species i in Zone j at C_j modulator concentration
L [cm] Column Length
Q_D [$mLmin^{-1}$] Desorbent liquid flow rate
Q_E [$mLmin^{-1}$] Extract liquid flow rate
Q_{Eq} [$mLmin^{-1}$] Equilibrium flow rate
Q_F [$mLmin^{-1}$] Feed liquid flow rate
Q_R [$mLmin^{-1}$] Raffinate liquid flow rate
Q_j [$mLmin^{-1}$] Liquid flow rate in Zone j
S_i [−] Coefficient for salt-dependency of partition for species i
t_2 [mins] Time for ideal solvent front to travel one column's distance in Zone2
t_S [mins] Switching Time
$v_{i,j}$ [cm/min] Velocity of species i in zone j
V [mL] Total Column Volume
V_0 [mL] Void volume of column
V_{Eq} [mL] Equilibration Volume
$V_{i,C_‡}$ [mL] Retention volume at transitional modulator concentration for species i
V_{i,C_M} [mL] Retention volume at a given modulator concentration for species i
V_{i,C_3} [mL] Retention volume at Zone 3 modulator concentration for species i
V_{lag} [mL] Lag volume for modulator due to non-plug-flow behavior
x_i [cm] Distance travelled by species i

Subscripts

i Feed species component, i=a,b
a Feed species "a", the more-retained component (MRC)
b Feed species "b", the less-retained component (LRC)
j Zone number, j=1:3 or j=1:4
C_M Relating to Modulator

Greek Letters

ε_{T,C_M} [−] Total void fraction available to modulator
$\varepsilon_{T,i}$ [−] Total void fraction available to species i
$\varepsilon_{p,i}$ [−] Particle porosity available to species i
φ_i [−] Phase ratio $\left(\frac{1-\varepsilon_{T,i}}{\varepsilon_{T,i}}\right)$ for species i

Ψ [−] The first MP dimensionless number
ω [min^{-1}] Port switching frequency
Ω_i [−] The second MP dimensionless number for species i

Keywords

design space, gradient SMB, modulator perturbation, robust design, simulated moving bed, stepwise-elution SMB, triangle theory

Received: October 24, 2017
Revised: March 15, 2018
Published online: June 4, 2018

[1] D.B. Broughton, C.G. Gerhold, US Patent 2985589, 1961.
[2] G. Storti, M. Mazzotti, M. Morbidelli, S. Carrl, *AIChE J*. **1993**, *39*, 471.
[3] G. Storti, R. Baciocchi, M. Mazzotti, M. Morbidelli, *Ind. Eng. Chem. Res*. **1995**, *34*, 288.
[4] D. C. S. Azevedo, A. E. Rodrigues, *AIChE J*. **1999**, *45*, 956.
[5] Z. Ma, N. Wang, *AIChE J*. **1997**, *43*, 2488.
[6] Y. Xie, D. Wu, Z. Ma, N. Wang, *Ind. Eng. Chem. Res*. **2000**, *39*.
[7] A. E. Rodrigues, L. S. Pais, *Sep. Sci. Technol*. **2004**, *39*, 245.
[8] M. Mazzotti, G. Storti, M. Morbidelli, *J. Chromatogr. A*. **1997**, *769*, 3.
[9] T. Mallmann, B. D. Burris, Z. Ma, N. Wang, *AIChE J*. **1998**, *44*, 2628.
[10] A. Tiselius, *Angew. Chem*. **1955**, *67*, 245.
[11] C. J. O. R. Morris, P. Morris, *Separation Methods in Biochemistry*, Halsted Press/Wiley, New York **1976**.
[12] T. B. Jensen, T. G. P. Reijns, H. A. H. Billiet, L. A. M. van der Wielen, *J. Chromatogr. A* **2000**, *873*, 149.
[13] P. Li, J. G. Yu, G. H. Xiu, A. E. Rodrigues, *Sep. Sci. Technol*. **2008**, *43*, 11.
[14] K. Temesvári, A. Aranyi, B. Csukás, S. Balogh, *Chromatographia* **2004**, *60*, 189.
[15] S. Mun, *J. Liquid Chromatogr. Related Technol*. **2011**, *34*, 1518.
[16] S. Abel, M. Mazzotti, M. Morbidelli, *J. Chromatogr. A* **2002**, *944*, 23.
[17] S. Abel, M. Mazzotti, M. Morbidelli, *J. Chromatogr. A* **2004**, *1026*, 47.
[18] L. C. Kessler, L. Gueorguieva, U. Rinas, A. Seidel-Morgenstern, *J. Chromatogr. A*. **2007**, *1176*, 69.
[19] S. Mun, L. Wang, *Process Biochem*. **2008**, *43*, 1407.
[20] L. Gueorguieva, S. Palani, U. Rinas, G. Jayaraman, A. Seidel-Morgenstern, *J. Chromatogr. A* **2011**, *1218*, 6402.
[21] J. Houwing, S. H. van Hateren, H. A. H. Billiet, L. A. M. van der Wielen, *J. Chromatogr. A* **2002**, *952*, 85.
[22] J. J. Lu, *Zheijang Univ. −Sci*. **2004**, *5*, 1613.
[23] P. C. Wankat, *Rate-Controlled Separations*, Blackie Academic & Professional, London UK **1994**.
[24] F. G. Helfferich, *Ion exchange*, McGraw-Hill, New York **1962**.
[25] A. Velayudhan, C. Horváth, *J. Chromatogr. A* **1994**, *663*, 1.
[26] A. Velayudhan, R. L. Hendrickson, M. R. Ladisch, *AIChE J*. **1995**, *41*, 1184.
[27] P. Jandera, J. Churáček, Gradient Elution in Column Liquid Chromatography: Theory and Practice, **1985**.
[28] G. Guichion, A. Felinger, D. G. Shirazi, A. Katti, *Fundamentals of Preparative and Nonlinear Chromatography*, 2nd edn., Elsevier Academic Press, San Diego, California, USA **2006**.
[29] Y. Kawajiri, L. T. Biegler, *Comp. Chem. Eng*. **2008**, *32*, 135.
[30] N. Taulier, T. V. Chalikian, *J. Mol. Biol*. **2001**, *314*, 873.
[31] E. J. Wilson, C. J. Geankoplis, *Ind. Eng. Chem. Fundam*. **1966**, *5*, 9.
[32] M. E. Young, P. A. Carroad, R. L. Bell, *Biotechnol. Bioeng*. **1980**, *22*, 947.
[33] S. F. Chung, C. Y. Wen, *AIChE J*. **1968**, *14*, 857.
[34] N. Graça, L. Pais, A. E. Rodrigues, *Chem. Eng.Technol*. **2015**, *38*, 2316.
[35] E. A. Borges da Silva, A. E. Rodrigues, *Sep. Sci. Technol*. **2008**, *43*, 533.
[36] E. A. Borges da Silva, A. E. Rodrigues, *AIChE J*. **2006**, *52*, 3794.
[37] F. Steinebach, T. Müller-Späth, M. Morbidelli, *Biotech J*. **2016**, *11*, 1126.

